# Crystallization of Isotactic Polypropylene under Shear Flow Observed in a Wide Spatial Scale

**Yoshiko Ogino, Hajime Fukushima, Nobuaki Takahashi,† Go Matsuba, Koji Nishida, and Toshiji Kanaya***

*Institute for Chemical Research, Kyoto University, Uji, Kyoto-fu 611-0011, Japan*

*Received June 6, 2006; Revised Manuscript Received August 21, 2006*

ABSTRACT: We studied crystallization process of isotactic polypropylene (iPP) under shear flow as a function of shear rate using time-resolved wide-angle X-ray scattering (WAXS), small-angle X-ray scattering (SAXS), depolarized light scattering (DPLS), and polarized optical microscopy (POM) to elucidate the formation mechanism of the so-called shish-kebab structure in a wide spatial scale from 0.1 nm to several tens of $\mu$m. In the time-resolved DPLS, SAXS, and WAXS measurements we observed the formation processes of the shish-like structure, the kebab structure, and the crystalline lattice (mostly in the kebab), respectively, and found that there were critical shear rates for the anisotropic structure formation in the DPLS, SAXS, and WAXS measurements. The values are very close each other, suggesting the anisotropic structure formations in both of the shish and the kebab are dominated by a common origin. Furthermore, comparing the onset times of intensities in DPLS, SAXS, and WAXS, we found that the onset of DPLS intensity is the most accelerated by the shear among the three. On the basis of the observations, we propose a possible mechanism for the shish-kebab structure.

## 1. Introduction

Molten polymers are subjected to various kinds of flows and temperature histories during processing such as spinning, injection molding, and extrusion; semicrystalline polymers crystallize during and/or after the flow, and the properties are strongly influenced by the final crystalline structure.[1−3] Therefore, extensive studies have been carried out on polymer crystallization under various flows such as shear flow and elongational flow both from scientific and industrial points of view to elucidate the crystallization mechanism under flows.[4] It is well-known that the so-called shish-kebab structure is often formed when semicrystalline polymers are crystallized under flows, which consists of a long central fiber core (shish) surrounded by lamellar crystalline structure (kebab) periodically attached along the shish, and it is believed that the shish-kebab structure is a molecular origin of ultrahigh strength and ultrahigh modulus fibers.[4−9] This is also one of the reasons why such many studies have been performed on polymer crystallization under flows. Although the previous studies have revealed the structure of shish-kebab in detail, there are still many unsolved problems in the formation mechanism. To control the structure and obtain desired properties, it is essential to understand the formation mechanism. On the basis of recent development of advanced characterization techniques, extensive studies have been performed on polymer crystallization under various kinds of flows using in situ rheo-small-angle and wide-angle X-ray scattering (SAXS and WAXS)[10−20] and in-situ rheo-small-angle light scattering (SALS)[21−25] and rheo-optical measurements,[26−28] providing fruitful information on the formation mechanism of shish-kebab structure. Combining the previous studies, it is expected that the shish-kebab structure has hierarchic structure in a wide spatial scale from 0.1 nm to several tens of $\mu$m.[22,24,29,30] It suggests that systematic studies in such a wide spatial scale must be essential to elucidate the relation between the shish and kebab formations. In this work, therefore, we have investigated crystallization process of isotactic polypropylene (iPP) under shear flow using WAXS, SAXS, depolarized LS (DPLS), and polarized optical microscopy (POM) techniques in order to see the formation of shish in $\mu$m scale, kebab in nm scale, and crystalline lattice formation (mostly in the kebab) in ∼0.1 nm scale, independently. The studies on shear rate effects for the shish and kebab formation allow us to estimate quantitatively critical shear rates for the anisotropic structure formation and the reduction in the induction time for each structure. These findings will show us an important role of relaxation of polymer chains in crystallization under shear flow.

## 2. Experimental Section

In the experiment we used isotactic polypropylene (iPP) with the molecular weight $M_w = 238\,000$ and the polydispersity $M_w/M_n = 5.1$, where $M_w$ and $M_n$ are the weight-average and number-average molecular weights, respectively. The iPP was synthesized using metallocene catalysis. Pentad tacticity determined by NMR measurements was *mmmm* = 0.974. DSC measurements were carried out to characterize the thermal properties of the sample using Perkin-Elmer DSC-7. All the DSC scans were performed under nitrogen environment. The nominal melting temperature of the iPP determined by DSC measurements was 149 °C at the heating rate of 20 °C/min.

Polarized optical microscopy (POM) measurements were carried out with an Olympus BX50 equipped with a CCD camera as a detector. Two-dimensional (2D) DPLS measurements were carried out using a homemade apparatus with He−Ne laser (80 mW, wavelength $\lambda = 633$ nm) as a light source and a 2D screen and a CCD camera as a detector system. The range of length of scattering vector $Q$ in this experiment is $3.5 \times 10^{-5}$−$3.0 \times 10^{-4}$ Å$^{-1}$, where $Q$ is given by $Q = 4\pi \sin\theta/n\lambda$ ($2\theta$ and $n$ being scattering angle and the refractive index, respectively).

Small-angle and wide-angle X-ray scattering (SAXS and WAXS) measurements were performed using apparatuses installed at the beamlines BL45XU[32] and BL40B2[33] in the SR facility, Spring-8, in Nishiharima, respectively. Wavelengths of the incident X-ray were 1.0 and 0.9 Å, and the camera lengths were 2.2 and 0.12 m for SAXS and WAXS, respectively. A CCD camera (C4880: Hamamatsu Photonics K.K.) with an image intensifier was used as a detector system for both the SAXS and WAXS measurements. The $Q$ range covered in the SAXS and WAXS measurements were 0.008−0.2 and 0.1−2.5 Å$^{-1}$, respectively.

* Corresponding author: Tel +81-774-38-3141; Fax +81-774-38-3146; e-mail kanaya@scl.kyoto-u.ac.jp.

† Present address: Quantum Beam Science Directorate, Japan Atomic Energy Agency, 2-4, Shirakatashirane, Tokai, Ibaraki 319-1195, Japan.

10.1021/ma061254t CCC: $33.50 © 2006 American Chemical Society
Published on Web 10/03/2006

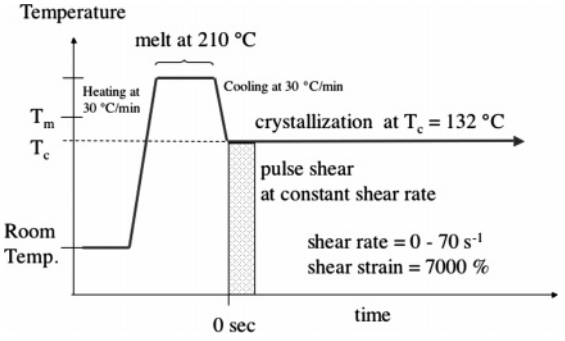


**Figure 1.** Temperature protocol for the shear experiments on iPP.

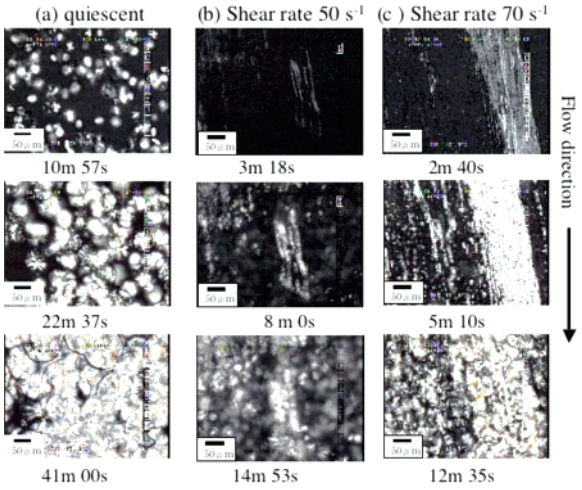


**Figure 2.** POM images during crystallization process of iPP under quiescent and shear conditions at 132 °C.

A Linkam CSS-450 high-temperature shear cell was used to control the temperature and the shear conditions. The sample thickness in the cell was 300 $\mu$m for the DPLS, SAXS, and WAXS measurements. The sample was placed between the two quartz plates for the POM and DPLS measurements and between two stainless steel plates with Kapton windows 50 $\mu$m thick for the SAXS and WAXS measurements, respectively. The temperature protocol for the shear experiments is shown in Figure 1: (a) the polymer sample was heated to 210 °C from room temperature at a rate of 30 °C/min, (b) held at 210 °C for 5 min, (c) cooled to the crystallization temperature $T_c$ = 132 °C at a rate of 30 °C/min, and then (d) held at 132 °C for the measurements. The polymer melt was subjected to pulse shear[31] just after reaching the crystallization temperature $T_c$ of 132 °C. The range of the shear rate was 0−70 $s^{-1}$, and the shear strain was 7000% at every shear rate.

## 3. Results and Discussion

**3.1. Polarized Optical Microscopy.** Polarized optical microscopy (POM) measurements were carried out on the crystallization process of iPP at 132 °C under quiescent and shear conditions after the temperature protocol described in the experimental part (see Figure 1). The results are shown in Figure 2 for the quiescent condition and the shear conditions with shear rates of 50 and 70 $s^{-1}$. The shear strains were 7000% for all the measurements. Under the quiescent condition, we observed growth of usual isotropic spherulites. The first spherulite appeared at about 5 min after reaching the crystallization temperature $T_c$ (=132 °C). On the other hand, under the shear conditions, stringlike structure or their bundles oriented along the flow direction appeared in the beginning of the crystallization. The onset time (or the induction time) of the stringlike structure is much shorter than that of the spherulites under the quiescent condition and becomes shorter with increasing the shear rate. The number of the strings also increases with the shear rate. In the late stage of crystallization isotropic spherulites were also observed even under the shear condition. These may come from some parts in the sample which were not affected by the shear or from the low molecular weight polymer chains which were relaxed before the crystallization.[4] The stringlike structure and their bundle must be the shish-kebab structure and/or their aggregates. These POM measurements give us intuitive images of the crystallization process under the quiescent and flow conditions. However, for the quantitative studies scattering methods are more appropriate than microscope measurements. Then, we performed time-resolved DPLS measurements.

**3.2. Depolarized Light Scattering.** Depolarized light scattering (DPLS) measurements were performed on the crystallization process of iPP under the same thermal history and the same shear conditions as the POM measurements (also see Figure 1). In this measurement, we can cover a range of scattering vector from 3.5 × $10^{-5}$ to 3.0 × $10^{-4}$ $Å^{-1}$, corresponding to a spatial scale of ∼18 to ∼2.0 $\mu$m. Hence, we will see the structure formation in $\mu$m scale, particularly the shish structure in the measurements. In Figure 3, time evolutions of 2D DPLS patterns are shown for various shear rates. The shear strains were 7000% for all the measurements. Under the quiescent crystallization condition ($\dot{\gamma}$ = 0 $s^{-1}$), we observed isotropic scattering pattern after an induction period before nucleation of about 5 min. This length of the induction period is almost identical with that for the spherulites in the POM measurements. On the other hand, as the shear rate increases, we observe anisotropic streaklike scattering pattern along the direction normal to the shear. This indicates that there are long scattering objects aligned along the flow direction, which must be the shish structure or the precursor of shish structure. At the moment it is not clear whether it is the shish structure or the precursor, and hence we call it the shish-like structure hereafter. The induction time and the anisotropy of the shish-like structure depend on the shear rate.

To analyze the DPLS data, we employed two measures. One is the length of the induction period before the streaklike scattering appears in the direction normal to the flow, which corresponds to the onset time of the shish-like structure. Another measure is the anisotropy in the 2D scattering pattern. First we discuss the length of the induction period. This is a sort of measure of the crystallization rate. Generally speaking, the crystallization rate is determined by both the nucleation rate and the growth rate.[34] The onset time is mainly related to the nucleation rate. In Figure 4, the integrated DPLS intensity normal to the flow direction in a $Q$ range of 0.35 × $10^{-4}$−2.5 × $10^{-4}$ $Å^{-1}$ (see also Figure 7) is plotted as a function of annealing time at 132 °C for various shear rates. We observe the onset of the scattering intensity after a certain induction period, which decreases with increasing the shear rate. The length of the induction period was estimated as the onset time of the integrated intensity as shown in Figure 4 for quiescent condition ($\dot{\gamma}$ = 0 $s^{-1}$) and was plotted against logarithm of the shear rate in Figure 5. The induction period decreases with increasing the shear rate, in particular, in the low shear rate range below about 7 $s^{-1}$. It seems there is a critical shear rate for the reduction in induction period $\dot{\gamma}^*_{ind,DPLS}$. However, it is hard to determine the critical shear rate precisely from the present data, but seems at around 1 $s^{-1}$.

Regarding the induction period, we have to emphasize the following problem. As mentioned in experimental part, pulse shear was applied to the sample just after reaching the

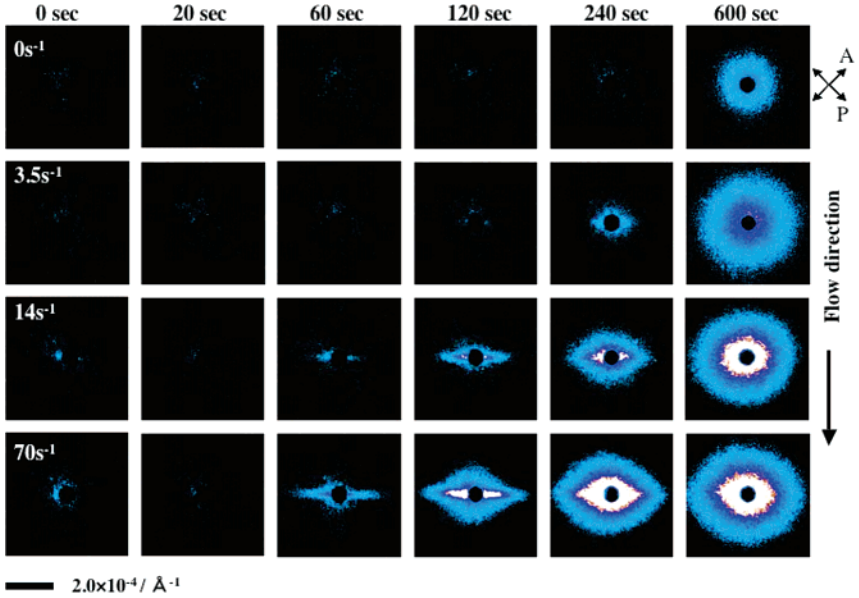


**Figure 3.** Time evolution of 2D DPLS patterns during crystallization process of iPP at 132 °C for various shear rates, $\dot{\gamma} = 0$, 3.5, 14, and 70 $s^{-1}$.

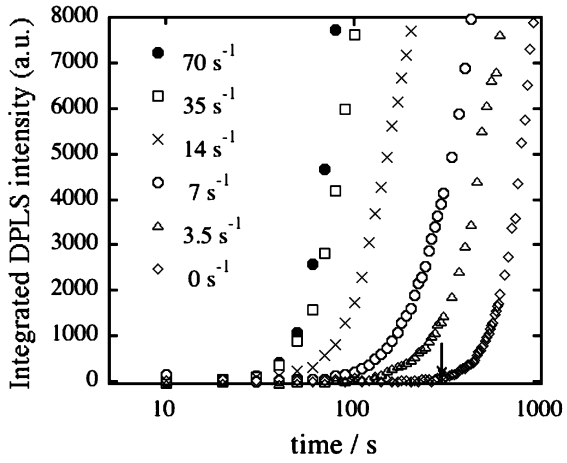


**Figure 4.** Time evolution of integrated intensity of DPLS normal to the flow direction during the crystallization process of iPP at 132 °C for various shear rates, $\dot{\gamma} = 0$, 3.5, 7, 14, 35, and 70 $s^{-1}$.

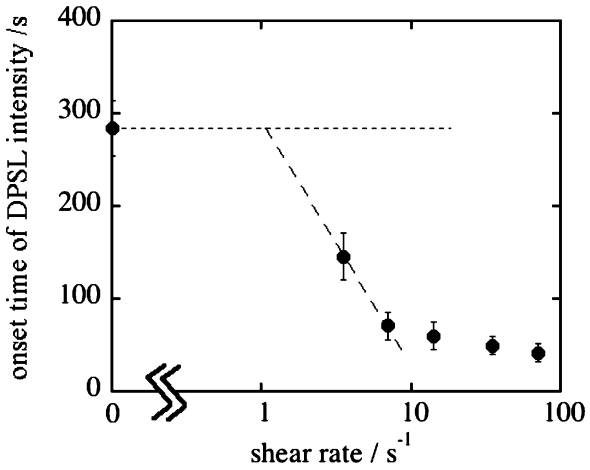


**Figure 5.** Onset time of integrated DPLS intensity normal to the flow direction as a function of shear rate.

crystallization temperature $T_c$ (=132 °C). During a few seconds after the pulse shear the detector screen of scattering light was bright, showing that bond orientation and/or chain orientation occurred due to the shear. The former and the latter occur in small and large scales, and the former relaxed much faster than

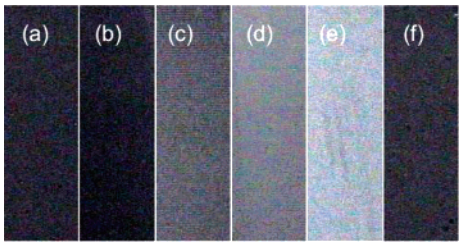


**Figure 6.** POM images before (a), during (b−e), and after (f) shearing for 1 s. (a) 1 s before application of the shear; (b) 0.25, (c) 0.5, (d) 0.75, and (e) 1.0 s after starting the shear; (f) 2 s after cessation of the shear. Shear rate is 70 $s^{-1}$ and shear direction is vertical.

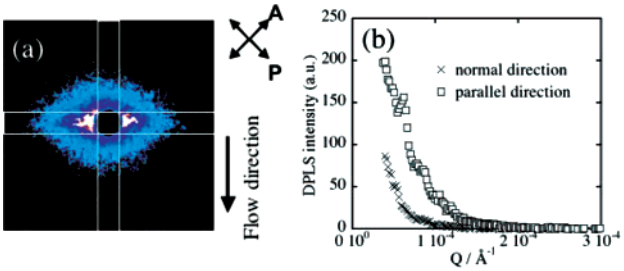


**Figure 7.** (a) Typical 2D DPLS pattern and (b) the intensity profiles in directions parallel and normal to the flow.

the latter.[35] Then, the screen became dark, suggesting that the orientations relaxed within a few seconds to be isotropic. However, the scattering pattern appearing after a certain induction time was anisotropic; i.e., streaklike scattering was observed in a direction normal to the flow, which means that there remain some oriented domains although we do not observe any sign of orientation in the present DPLS measurements in the induction period. To investigate this phenomenon, we performed polarized optical microscopy (POM) measurements, which is mainly governed by the bond orientation, before and after applying pulse shear with shear rate of 70 $s^{-1}$. The result is shown in Figure 6. The POM image just before the pulse shear was completely dark. During application of the shear (1 s) the POM image gradually became bright, showing that the bond orientation proceeds. On the other hand, it became dark soon (<2 s) after cessation of the shear, showing that the bond oriented relaxed soon. This result means that the bond orientation is not a main reason for the anisotropic structure formation

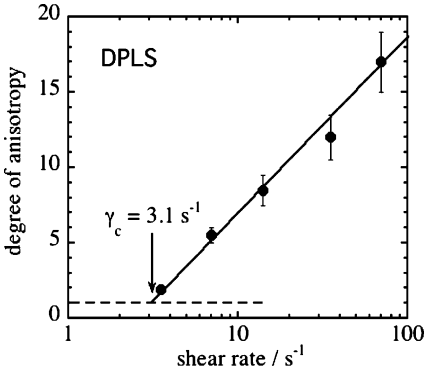


**Figure 8.** Degree of anisotropy for 2D DPLS patterns of iPP as a function of shear rate.

after the induction period. Probably there remain some hidden chain orientations, which are governed by the reptation motion,[35] and the chain orientation makes the subsequent structure development anisotropic. At the moment, however, we have no answer to this hidden chain orientation.

The second measure is a degree of anisotropy in the 2D scattering pattern. A typical 2D DPLS pattern is shown in Figure 7a. As a measure of the anisotropy of the scattering pattern, we employed a ratio of integrated intensity in the normal direction to the parallel one in the $Q$ range of $0.35 \times 10^{-4}-2.5 \times 10^{-4}$ Å$^{-1}$ (see Figure 7b) and termed the degree of anisotropy $R_{ani}$. It is noted that the degree of anisotropy can be defined only after the induction period of the scattering intensity. After the induction period, it is almost constant for a while and began to decrease with annealing time. This decrease is due to the appearance of isotropic spherulites, as seen in the POM pictures in Figure 2. Then, we used the constant value of the degree of anisotropy $R_{ani}$ in the following discussion.

The degree of anisotropy $R_{ani}$ is plotted against logarithm of the shear rate in Figure 8. It increases linearly with logarithm of the shear rate above a certain critical shear rate $\dot{\gamma}^*_{ani,DPLS}$ in the present shear rate range. This relation can be written in the following form:

$$\dot{\gamma}^*_{ani,DPLS} = \dot{\gamma} \exp\left[-\frac{R_{ani} - R_{ani,0}}{r_{ani}}\right] \quad (1)$$

where $\dot{\gamma}^*_{ani,DPLS}$, $R_{ani,0}$, and $r_{ani}$ are the critical shear rate for the anisotropy, the degree of anisotropy under quiescent condition (=1), and a dimensionless constant. The critical shear rate $\dot{\gamma}^*_{ani,DPLS}$ was evaluated to be $3.1 \pm 0.3$ s$^{-1}$ by extrapolating the degree of anisotropy to unity. The critical shear rate for the degree of anisotropy $\dot{\gamma}^*_{ani,DPLS}$ is larger than that for the induction period $\dot{\gamma}^*_{ind,DPLS}$. Similar results were reported for polyethylene.[24] The physical meaning of the finding will be discussed later.

In the above DPLS measurements we observed the formation process of the shish-like structure in a spatial scale of $\mu$m. It is noted that shish with ~10 nm diameter was reported in transmitted electron microscopy (TEM) measurements.[29] Recently, we performed small-angle neutron scattering (SANS) measurements on an elongated blend of deuterated polyethylene (PE) with normal molecular weight ($M_w$ = ~200 000) including a small amount of protonated ultrahigh molecular weight PE ($M_w$ = 2 000 000, 2.8 wt %). The result shows that there exist shishs with diameter of ~10 nm in addition to the shish-like structure in $\mu$m scale observed in the DPLS, suggesting hierarchic structure of shish. This problem will be discussed in a forthcoming paper.

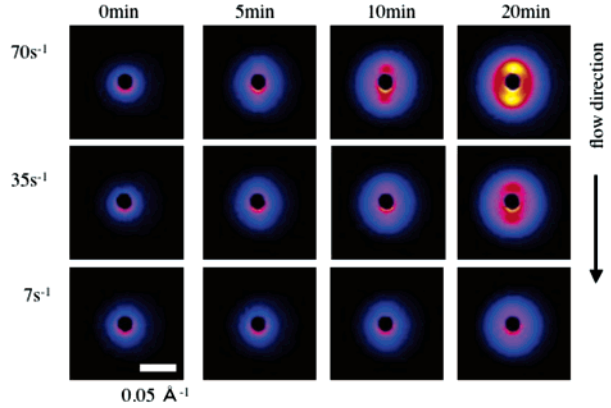


**Figure 9.** Time evolution of 2D SAXS patterns during crystallization process of iPP at 132 °C for various shear rates, $\dot{\gamma}$ = 7, 37, and 70 s$^{-1}$.

Next we have performed time-resolved small-angle X-ray scattering measurements on the crystallization process of the same iPP in hundreds nm scale in order to see the formation process of the kebab structure.

**3.3. Small-Angle X-ray Scattering.** Time-resolved small-angle X-ray scattering (SAXS) measurements were carried out on crystallization process of iPP under the same temperature and shear conditions as the DPLS. The same iPP was heated to 210 °C and held for 5 min and then cooled to the crystallization temperature $T_c$ = 132 °C at a cooling rate of 30 °C/min. Just after reaching $T_c$, pulse shear was applied, and the time-resolved SAXS measurements were carried out at 132 °C. The shear rates were in a range of 0−70 s$^{-1}$, and the shear strain was 7000% for all the measurements. The observed time evolution of 2D SAXS patterns is shown in Figure 9 for the shear rates of 7, 35, and 70 s$^{-1}$. Under the quiescent condition, only isotropic scattering patterns were observed, and the onset time of the scattering intensity is about 650 s after reaching the crystallization temperature $T_c$ (=132 °C). On the other hand, under the shear condition, the onset time of the scattering intensity is earlier than that under the quiescent condition, and the scattering pattern is anisotropic. For example, at the shear rate of 70 s$^{-1}$, weak streaklike scattering intensity appears along the flow direction at about 60 s after applying the pulse shear, and the scattering pattern gradually becomes a two-spot pattern. In addition to this, isotropic scattering ring also appears in the late stage of the crystallization. The anisotropic SAXS pattern is completely different from the DPLS one (see Figure 3), in which streaklike scattering appears in a direction normal to the flow. The observed two-spot SAXS pattern parallel to the flow direction must correspond to the distance between the lamellae (kebabs) periodically aligned along the shish structure. To analyze these SAXS data quantitatively, we also used the onset time and the degree of anisotropy, which depend on the shear rate very much.

The time evolution of the integrated scattering intensity parallel to the flow direction in a $Q$ range of 0.015−0.05 Å$^{-1}$ is shown in Figure 10 for the shear rates of 0, 7, 14, and 70 s$^{-1}$. The onset time was defined as a rise-up time of the integrated scattering intensity in a direction parallel to the flow as shown by an arrow for the quiescent condition. The estimated onset time is plotted against logarithm of the shear rate in Figure 11. In the low shear rate region, it decreases drastically with increasing the shear rate, showing large effects of the shear rate on the crystallization rate. From the present data, it is hard to determine precisely the critical shear rate for the reduction in the induction time $\dot{\gamma}^*_{ind,DPLS}$, but seems at around 1 s$^{-1}$.

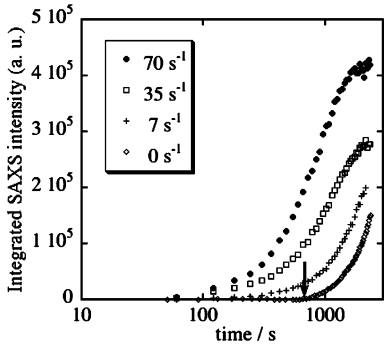


**Figure 10.** Time evolution of integrated intensity of SAXS parallel to the flow direction during the crystallization process of iPP at 132 °C for various shear rates, $\dot{\gamma} = 0$, 7, 35, and 70 $s^{-1}$.

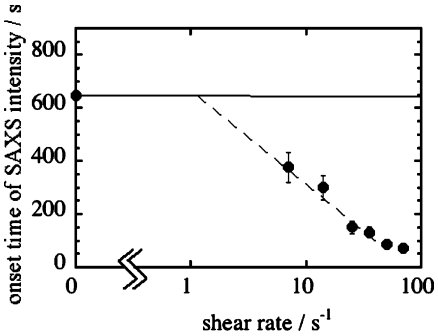


**Figure 11.** Onset time of integrated SAXS intensity parallel to the flow direction as a function of shear rate.

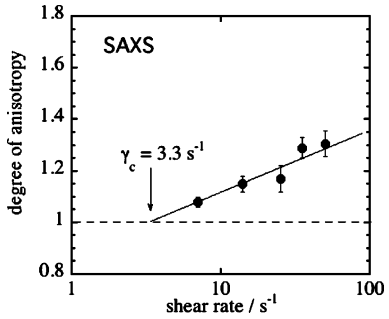


**Figure 12.** Degree of anisotropy for 2D SAXS patterns of iPP as a function of shear rate.

We defined the degree of anisotropy for the 2D SAXS pattern as a ratio of integrated intensity parallel to the flow direction to the normal one. The ratio cannot be calculated in the induction period and fluctuates very much just after the induction period because of the weak intensity. The ratio becomes stable and almost constant in a period before the isotropic scattering appears. Hence, we employed the ratio in the stable region as the degree of anisotropy, which was plotted in Figure 12 against logarithm of the shear rate. Assuming a linear relationship between the degree of anisotropy and the logarithm of the shear rate below 35 $s^{-1}$, we extrapolated the degree of anisotropy to unity to evaluate the critical shear rate $\dot{\gamma}^*_{ani,DPLS}$ to be $3.3 \pm 0.6$ $s^{-1}$. The error was estimated from the upper and lower slopes in the extrapolation. This value is larger than the critical shear rate for the reduction in the induction period $\dot{\gamma}^*_{ind,SAXS}$ ($\sim$1 $s^{-1}$). The critical shear rate for the anisotropy $\dot{\gamma}^*_{ani,SAXS}$ evaluated in the SAXS (or the kebab) (=3.3 $s^{-1}$) is close to that in the DPLS (the shish) $\dot{\gamma}^*_{ani,DPLS}$ (=3.1 $s^{-1}$). This must imply that the anisotropy of the kebab structure is dominated by the shish formation. This problem will be discussed later after showing the wide-angle X-ray scattering results.

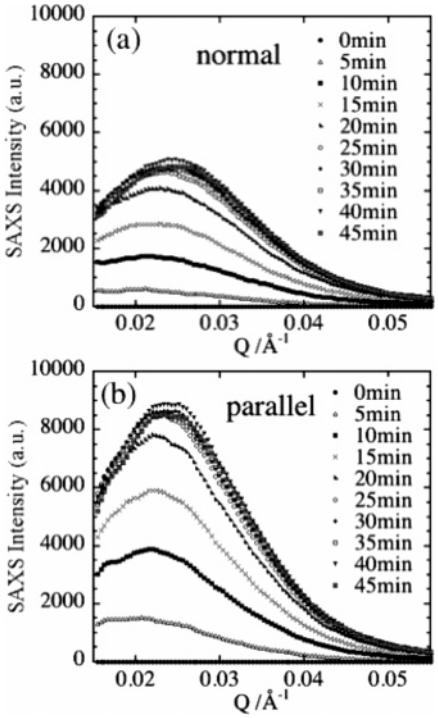


**Figure 13.** Time evolution of 1D SAXS profiles normal (a) and parallel (b) to the flow.

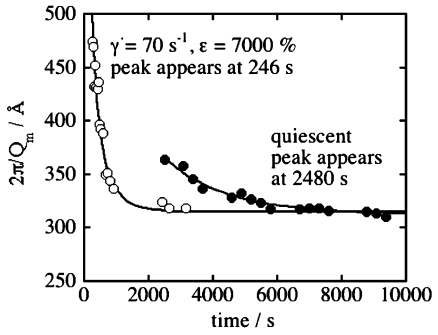


**Figure 14.** Time evolution of long period evaluated from the peak positions $Q_m$ in through $2\pi/Q_m$ during the crystallization of iPP at 132 °C under quiescent and shear condition ($\dot{\gamma} = 70$ $s^{-1}$).

The $Q$ dependence of the scattering intensities normal and parallel to the flow direction are shown in parts a and b of Figure 13, respectively. The peak position $Q_m$ of the scattering intensity parallel to the flow direction gives us the spacing between the kebab structure aligned along the shish structure. The spacing evaluated from $2\pi/Q_m$ is plotted as a function of the annealing time for the shear rate of 70 $s^{-1}$ in Figure 14 where the lamella spacing under the quiescent crystallization condition is also plotted. In the quiescent condition, the peak is first recognized at around 2500 s after induction period of about 650 s, and the spacing is about 360 Å, which gradually decreases with annealing time to reach about 310 Å. On the other hand, under the shear condition of 70 $s^{-1}$ the scattering peak is recognized at about 250 s after the pulse shear, which is much earlier than the quiescent condition. The initial spacing (=475 Å) is longer than the quiescent condition (360 Å) and becomes smaller to level off at 320−310 Å, which is almost the same as the final value under the quiescent condition. The earlier appearance of the peak shows the acceleration of the crystallization rate under the shear. This must be caused by epitaxial secondary nucleation on the shish structure. The large initial value of the lamella spacing under the shear must show that lamellae (the kebabs) grow site-randomly on the shish, but not regularly one by one

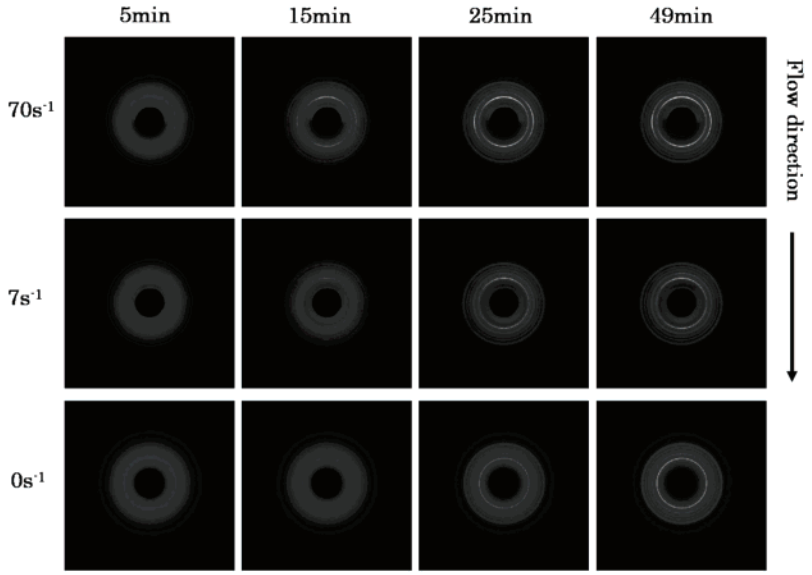


**Figure 15.** Time evolution of 2D WAXS patterns during crystallization process of iPP at 132 °C for various shear rates, $\dot{\gamma} = 0$, 7, and 70 $s^{-1}$.

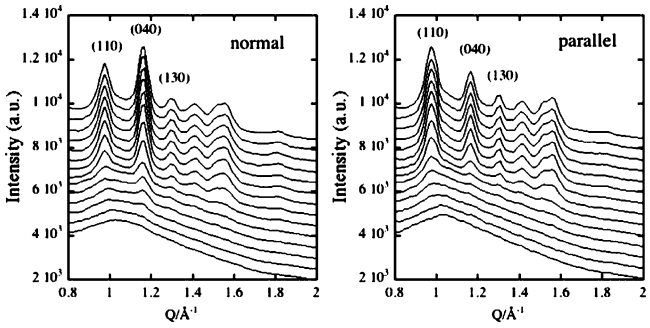


**Figure 16.** Time evolution of 1D WAXS profiles normal and parallel to the flow direction after cessation of the shear with shear rate of 70 $s^{-1}$. The profiles were shifted vertically for clarification. Annealing times after pulse shear are 0, 2, 4, 6, 8, 10, 15, 20, 25, 30, 35, 40, 45, and 50 min from bottom to top for both parallel and normal directions.

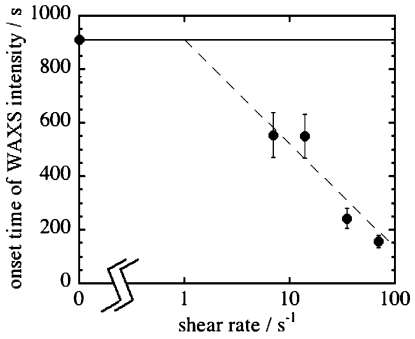


**Figure 17.** Onset time of (040) diffraction intensity parallel to the flow direction as a function of shear rate.

on the shish. However, the identical final spacing between the quiescent and shear conditions implies that the spacing is not determined by the shear effects.

**3.4. Wide-Angle X-ray Scattering.** Time-resolved wide-angle X-ray scattering (WAXS) measurements were performed on the same iPP under the same temperature and shear conditions as the DPLS and SAXS measurements. The crystallization temperature $T_c$ was 132 °C, and the shear strain was 7000% for all the measurements. In the WAXS measurements we observed the time evolution of the local crystalline structure in both of the shish and the kebab, particularly in the kebab because the amount of kebab is much larger than the shish.[25] In fact, the WAXS intensity from the shish is not recognized within the present WAXS sensitivity. Time evolution of 2D WAXS patterns is shown in Figure 15 for the shear rates of 0, 7, and 70 $s^{-1}$. The scattering patterns are isotropic under the quiescent condition while it is anisotropic under the shear condition. The anisotropic time evolution of 1D WAXS profiles normal and parallel to the shear direction are shown in parts a and b of Figure 16, respectively, for the shear rate of 70 $s^{-1}$. In the figures the intensities are shifted vertically for clarification. The diffraction patterns show that the crystal has mainly α-form, including a small amount of $\gamma$-form and the intensity must be from the kebab. The diffraction intensity from the (040) plan is larger in the normal direction than in the parallel direction, suggesting that the *b*-axis of the lamella (the kebab) aligns normal to the shear direction and is the growth direction. The (110) diffraction intensity is larger in the parallel direction than in the normal direction, and hence it is expected that the *a*-axis rotates around the *b*-axis during the kebab growth. As seen in parts a and b of Figure 16, the (040) and (110) diffraction intensities appear earlier in the normal and parallel directions to the flow, respectively, and followed by the intensities in the parallel and normal directions, respectively. This suggests that the kebab grows in a particular direction (along the *b*-axis) in the early stage and followed by the isotropic spherulites as observed in the optical microscope measurements. In fact, the onset time of the (040) diffraction intensity in the parallel direction is close to the onset of the isotropic spherulites under quiescent states (~900 s). In Figure 17, the onset time of the (040) intensity is plotted as a function of the shear rate. Similar to the DPLS and SAXS cases, it is hard to decide precisely the critical shear rate for the reduction in the induction period $\dot{\gamma}^*_{ind,WAXS}$. If we extrapolate the linear relation shown in Figure 17 to the induction time under quiescent condition, the critical shear rate $\dot{\gamma}^*_{ind,WAXS}$ is at around 1 $s^{-1}$ although large error must be allowed in this estimation.

The degree of anisotropy for the (040) diffraction intensity was defined as an intensity ratio of the normal direction to the parallel one after subtracting the melt intensity at $t = 0$ and is plotted in Figure 18 against logarithm of the shear rate. Although the data points rather scattered, there certainly exists a critical shear rate for the anisotropy $\dot{\gamma}^*_{ani,WAXS}$ or for the crystal lattice formation in the kebab. Extrapolating the data to the degree of anisotropy of unity, we have evaluated the critical shear rate $\dot{\gamma}^*_{ani,WAXS}$ to be 3.3 ± 0.5 $s^{-1}$, which is larger than the critical

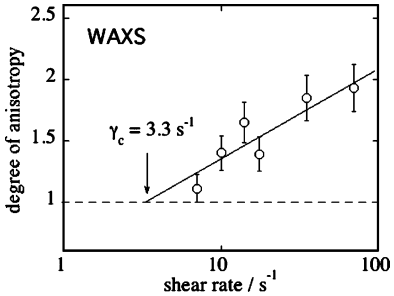


**Figure 18.** Degree of anisotropy for 2D WAXS patterns of iPP as a function of shear rate.

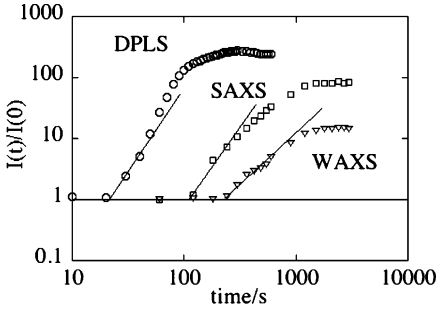


**Figure 19.** Comparison of time evolution of DPLS, SAXS, and WAXS intensities during crystallization process of iPP at 132 °C after pulse shear with shear rate of 70 $s^{-1}$.

shear rate for the reduction in the induction period $\dot{\gamma}^*_{ind,WAXS}$, similar to the cases of the DPLS and SAXS experiments. The value of 3.3 $s^{-1}$ is rather close to the critical values for the anisotropic structure formations in DPLS (=3.1 $s^{-1}$) and in SAXS (= 3.3 $s^{-1}$) ($\dot{\gamma}^*_{ani,DPLS} \approx \dot{\gamma}^*_{ani,SAXS} \approx \dot{\gamma}^*_{ani,WAXS} \approx 3.2\ s^{-1}$), suggesting that the anisotropic structure formation is dominated by a common origin. These values are larger than the critical shear rates for the induction period evaluated in DPLS, SAXS, and WAXS measurements ($\dot{\gamma}^*_{ind,DPLS} \approx \dot{\gamma}^*_{ind,SAXS} \approx \dot{\gamma}^*_{ind,WAXS} \approx 1\ s^{-1}$). In the following we discuss the formation mechanism on the basis of these data.

**3.5. Comparison of DPLS, SAXS, and WAXS Data and Formation Mechanism of Shish-Kebab Structure.** The time evolutions of the scattering intensities are compared among the DPLS, SAXS, and WAXS measurements. The intensities of DPLS, SAXS, and WAXS are shown as a function of annealing time after applying pulse shear with shear rate of 70 $s^{-1}$ at 132 °C in Figure 19, where the intensities were normalized to the initial intensity at $t = 0$ s and plotted in double-logarithmic form. This plot was done to show the earliest onsets of the intensities more clearly than log−linear plots of intensities such as Figures 4 and 10.

It is very clear that the DPLS intensity rises up the earliest at around 20 s, the SAXS intensity is next at 100 s, and finally the WAXS intensity comes at around 140 s. When we compare intensities obtained by different scattering methods, we have to take into account the difference of sensitivities. During the crystallization process at 132 °C under quiescent condition, we observed the onset of DPLS, SAXS, and WAXS intensities at about 300, 650, and 900 s, respectively. These onset times reflect the difference of the sensitivities involving structure factor, scattering contrast, counter efficiency, noise-to-signal ratio, etc., and hence it is difficult to compare them directly. To compare the results, we took the ratio of the onset time under quiescent to that under shear for each scattering method, which gives 15 (=300/20), 6.5 (=650/100), and 6.4 (=900/140) for DPLS, SAXS, and WAXS, respectively. The largest ratio of 15 indicates that the shish-like structure formation observed in DPLS is the most accelerated by shear, suggesting that the shish-like structure is formed first. The ratios for SAXS and WAXS are almost the same and smaller than for DPLS, meaning that the acceleration of the kebab structure formation by the flow is less than the shish-like structure. In other words, the shish-like structure is formed earlier than the kebab. On the other hand, it is very interesting to point out that the critical shear rate for the anisotropic structure formation is almost the same for DPLS, SAXS, and WAXS, which are 3.1 ± 0.3, 3.3 ± 0.6, and 3.3 ± 0.5 $s^{-1}$, respectively: $\dot{\gamma}^*_{ani,DPLS} \approx \dot{\gamma}^*_{ani,SAXS} \approx \dot{\gamma}^*_{ani,WAXS}$ ($\equiv \dot{\gamma}^*_{ani}$). How can we understand the results? The ratio of the onset times implies that the shish-like structure oriented along the flow is formed first, and then the lamella (kebab) may be epitaxially formed on the surface of shish-like structure, resulting in the oriented lamella structure or the kebab structure. If the oriented shish-like structure is not formed in the weak shear rate range below the critical value $\dot{\gamma}^*_{ani,DPLS}$, it would be impossible to form the oriented kebabs. In other words, the critical shear rate for the anisotropic shish-like structure formation governs the orientation of the kebab.

Finally, we consider why the critical shear rate for the reduction in induction time $\dot{\gamma}^*_{ind}$ is smaller than that for the anisotropic structure $\dot{\gamma}^*_{ani}$. A schematic illustration for the shish-kebab formation is given in Figure 20 for explanation. In the low shear rate region below the critical value for the reduction in the induction time ($\dot{\gamma} < \dot{\gamma}^*_{ind}$), polymer chains are somewhat extended to orient by the shear (Figure 20a-1). If crystallization occurs in the oriented state, the crystallization rate must be faster than that under quiescent state. However, in the low shear rate rage we did not observe any acceleration of crystallization rate, suggesting that the orientation must relax to be isotropic before nucleation (Figure 20a-2). In this case, crystallization occurs in isotropic melt and acceleration of crystallization would not be observed (Figure 20a-3,4). In the shear rate region above the critical shear rate for the reduction in the induction time and below the critical shear rate for the anisotropic structure formation ($\dot{\gamma}^*_{ind} < \dot{\gamma} < \dot{\gamma}^*_{ani}$), crystal nucleation must occur before the relaxation of the orientation (Figure 20b-2), and the nucleation rate is accelerated due to the orientation (orientation-induced crystallization). This acceleration is in a small orientation domain because the so-called primary nuclear is in a size of ∼15 nm.[36] On the other hand, for the shish-like structure formation, the crystal growth must occur along the oriented chains or new crystal nuclei must be formed along the chains (or the segments) to prevent the relaxation of chain orientation. In this shear rate region, therefore, it is expected that the chain orientation is relaxed in global scale (∼$\mu$m) before the crystal growth occurs along the chains (Figure 20b-3). Above the critical shear rate for the anisotropic structure formation ($\dot{\gamma}^*_{ani} < \dot{\gamma}$), on the other hand, nucleation rate of polymer chains oriented by the shear is accelerated due to the orientation (Figure 20c-2) and the crystal growth in the large scale occurs before the relaxation of chain orientation, resulting in the anisotropic shish-like structure (Figure 20c-3). The chain orientation is mainly governed by reptation motion,[35] suggesting that entanglements of polymer chains play an important role, and the critical shear rate $\dot{\gamma}^*_{ani}$ is in the order of inverse of the reptation time. Folded chain lamella crystals (kebabs) grow on the surface of the shish to form the shish-kebab structure (Figure 20c-4). It is expected that the kebab grows epitaxially on the surface of the shish-like structure, and hence the acceleration of the shish growth accelerates the kebab growth and the anisotropic shish-like structure induces the anisotropic kebab formation (Figure 20c-3,4). Therefore, it

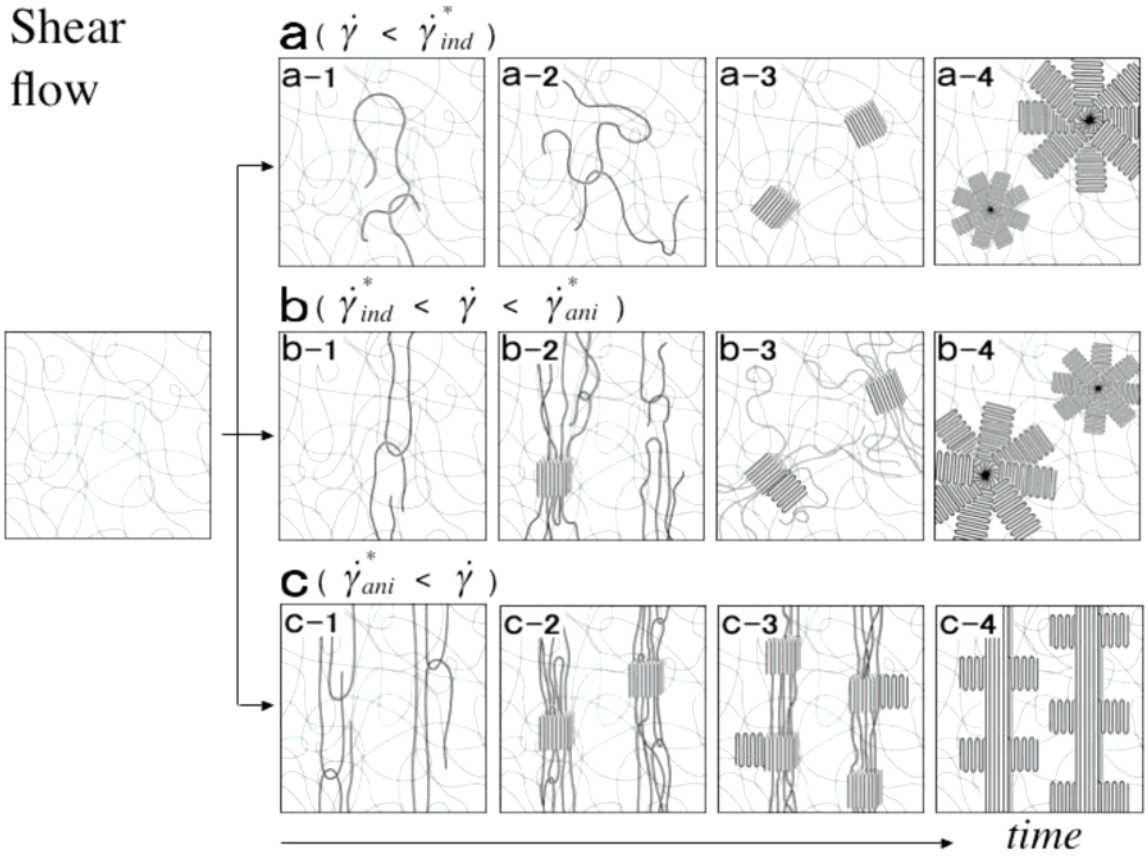


**Figure 20.** Schematic illustration for the shish-kebab formation: (a) shear rate region below the critical value for the reduction in the induction time ($\dot{\gamma} < \dot{\gamma}^*_{ind}$); (b) shear rate region above the critical shear rate for the reduction in the induction time and below the critical shear rate for the anisotropic structure formation ($\dot{\gamma}^*_{ind} < \dot{\gamma} < \dot{\gamma}^*_{ani}$); (c) shear rage region above the critical shear rate for the anisotropic structure formation ($\dot{\gamma}^*_{ani} < \dot{\gamma}$). Thick lines represent oriented polymer chains.

is not surprising that the critical shear rates are almost identical between the kebab and shish-like structure for the reduction in the induction time as well as for the anisotropic structure formation.

## 4. Conclusion

In this study we have investigated crystallization process of iPP after applying pulse shear in a wide spatial scale from 0.1 nm to several tens of $\mu$m using time-resolved DPLS, SAXS, WAXS, and POM techniques. It was found that there were two critical shear rates: one is for the reduction in the induction time before nucleation $\dot{\gamma}^*_{ind}$, and the other is for the anisotropic structure formation $\dot{\gamma}^*_{ani}$. The former critical shear rate is always smaller than the latter one. It was also found that the critical shear rates for the anisotropic structure formation are almost identical for DPLS, SAXS, and WAXS whether it sees the shish-like formation or the kebab formation. In addition, we found that the shish-like structure formation is accelerated by the shear more than the kebab formation, suggesting that the shish-like structure is formed before the kebab under the shear flow. On the basis of these observations, we proposed a possible scenario for the shish-kebab structure. After applying pulse shear polymer chains (or segments) are extended and oriented, and hence the nucleation rate is accelerated by the orientation (orientation-induced nucleation). If the shear rate is large enough that the successive nucleation occurs along the oriented chains to overcome the chain relaxation, the anisotropic shish-like structure is formed. This means that the shish-like structure formation is dominated by a competition between the nucleation rate and the chain relaxation rate. Once the shish-like structure is formed above the critical shear rate for the anisotropic structure formation, lamella crystals could grow epitaxially on the surface of the shish-like structure. In other words, the anisotropic structure formation of kebab is dominated by the shish-like structure formation, and hence the critical shear rates for the anisotropic shish-like and kebab structure formations are almost identical.

**Acknowledgment.** We are indebted to Prof. K. Kaji for variable discussions. We are also grateful to Dr. T. Fujisawa for support of X-ray scattering experiments on a beamline BL45XU in Spring-8 and to Dr. K. Inoue and Dr. S. Sasaki on a beamline BL40B2 in Spring-8.

## References and Notes

(1) Ward, I. M. *Structure and Properties of Oriented Polymers*; Wiley: New York, 1975.
(2) Ziabicki, A. *Fundamentals of Fiber Formation*; Wiley: New York, 1976.
(3) Walczak, Z. K. *Processses of Fiber Formation*; Elsevier: Amsterdam, 2002.
(4) Keller, A.; Kolnaar, J. W. H. In *Processing of Polymers*; Meijer, H. E. H., Ed.; VCH: New York, 1997; pp 189−268.
(5) Pennings, A. J.; Kiel, A. M. *Colloid Z. Z. Polym.* **1965**, *205*, 160−162.
(6) Pennings, A. J. *J. Polym. Sci., Part C: Polym. Symp.* **1977**, *59*, 55−86.
(7) Odell, J. A.; Grubb, D. T.; Keller, A. *Polymer* **1978**, *19*, 617−626.
(8) Bashir, Z.; Odell, J. A.; Keller, A. *J. Mater. Sci.* **1984**, *19*, 3713−3725.
(9) Bashir, Z.; Odell, J. A.; Keller, A. *J. Mater. Sci.* **1986**, *21*, 3993−4002.
(10) Samon, J. M.; Schultz, J. M.; Hsiao, B. S.; Seifert, S.; Stribeck, N.; Gurke, I.; Collins, G.; Saw, C. *Macromolecules* **1999**, *32*, 8121−8132.
(11) Samon, J. M.; Schultz, J. M.; Wu, J.; Hsiao, B. S.; Yeh, F.; Kolb, R. *J. Polym. Sci., Part B: Polym. Phys.* **1999**, *37*, 1277−1287.

(12) Somani, R. H.; Hsiao, B. S.; Nogales, A.; Srinivas, S.; Tsuo, A. H.; Sics, I.; Balta-Calleja, J.; Ezquerra, T. A. *Macromolecules* **2000**, *33*, 9385−9394.
(13) Schultz, J. M.; Hsiao, B. S.; Samon, J. M. *Polymer* **2000**, *41*, 8887−8895.
(14) Samon, J. M.; Schultz, J. M.; Hsiao, B. S.; Wu, J.; Khot, S. *J. Polym. Sci., Part B: Polym. Phys.* **2000**, *38*, 1872−1882.
(15) Samon, J. M.; Schultz, J. M.; Hsiao, B. S.; Khot, S.; Johnson, H. R. *Polymer* **2001**, *42*, 1547−1559.
(16) Nogales, A.; Somani, R. H.; Hsiao, B. S.; Srinivas, S.; Tsuo, A. H.; Balta-Calleja, J.; Ezquerra, T. A. *Polymer* **2001**, *42*, 5247−5256.
(17) Somani, R. H.; Hsiao, B. S.; Nogales, A.; Fruitwala, H.; Srinivas, S.; Tsuo, A. H. *Macromolecules* **2001**, *34*, 5902−5909.
(18) Somani, R. H.; Young, L.; Hsiao, B. H.; Agarwal, P. K.; Fruitwala, H. A.; Tsuo, A. H. *Macromolecules* **2002**, *35*, 9096−9104.
(19) Somani, R. H.; Yang, L.; Hsiao, B. S. *Physica A* **2002**, *304*, 145−157.
(20) Yang, L.; Somani, R. H.; Sics, I.; Hsiao, B. H.; Kolb, R.; Fruitwala, H.; Ong, C. *Macromolecules* **2004**, *37*, 4845−4859.
(21) Pogodina, N. V.; Siddiquee, S. K.; Egmond, J. W. v.; Winter, H. H. *Macromolecules* **1999**, *32*, 1167−1174.
(22) Pogodina, N. V.; Lavrenko, V. P.; Srinivas, S.; Winter, H. H. *Polymer* **2001**, *42*, 9031−9043.
(23) Elmoumni, A.; Winter, H. H.; Waddon, A. J.; Fruitwala, H. *Macromolecules* **2003**, *36*, 6453−6461.
(24) Fukushima, H.; Ogino, Y.; Matsuba, G.; Nishida, K.; Kanaya, T. *Polymer* **2005**, *46*, 1878−1885.
(25) Ogino, Y.; Fukushima, H.; Matsuba, G.; Takahashi, N.; Nishida, K.; Kanaya, T. *Polymer* **2006**, *47*, 5669.
(26) Kumaraswamy, G.; Issaian, A. M.; Kornfield, J. A. *Macromolecules* **1999**, *32*, 7537−7547.
(27) Kumaraswamy, G.; Verma, R. K.; Issaian, A. M.; Wang, P.; Kornfield, J. A.; Yeh, F.; Hsiao, B.; Olley, R. H. *Polymer* **2000**, *41*, 8934−8940.
(28) Kumaraswamy, G.; Kornfield, J. A.; Yeh, F.; Hsiao, B. *Macromolecules* **2002**, *35*, 1762−1769.
(29) Bashir, Z.; Hill, M. J.; Keller, A. *J. Mater. Sci., Lett.* **1986**, *5*, 876−878.
(30) Hsiao, B.; Yang, L.; Somami, R. H.; Avila-Orta, C. A.; Zhu, L. *Phys. Rev. Lett.* **2005**, *94*, 117802-1−118902-4.
(31) Fujisawa, T.; Inoue, K.; Oka, T.; Iwamoto, H.; Uruga, T.; Kumasaka, T.; Inoko, Y.; Yagi, N.; Yamamoto, M.; Ueki, T. *J. Appl. Crystallogr.* **2000**, *33*, 797.
(32) Shimizu, N.; Inoue, K. *SPring-8 Beamline Handbook* **2003**, 90.
(33) Jerschow, P.; Janeschitz-Kriegel, H. *Int. Polym. Process* **1997**, *12*, 72−77.
(34) Mandelkern, L. *Crystallization of Polymers—Kinetics and Mechanisms*; Cambridge Univesity Press: Cambridge, 2002.
(35) Bent, J.; Hutchings, L. R.; Richards, R. W.; Gough, T.; Spares, R.; Coates, P. D.; Grillo, I.; Harlen, O. G.; Read, D. J.; Graham, R. S.; Liktman, A. E.; Groves, D. J.; Nicholson, T. M.; Mcleish, T. C. B. *Science* **2003**, *301*, 1691.
(36) Wunderlich, B. *Macromolecular Physica—Crystal Nucleation, Growth, Annealing*; Academic Press: New York, 1976.

MA061254T